

Low Velocity Impacts into Dust:  
Results from the COLLIDE-2 Microgravity Experiment

Joshua E. Colwell  
Laboratory for Atmospheric and Space Physics  
University of Colorado, Campus Box 392  
Boulder CO 80309-0392  
(303) 492-6805  
(303) 492-6946 (FAX)  
josh.colwell@lasp.colorado.edu

February 12, 2003

Submitted to *Icarus*: 2002  
Revised: February 12, 2003  
Manuscript pages: 23  
Figures: 7  
Tables: 2

Suggested running head: Low Velocity Microgravity Impact Experiments

Address correspondence to:

Joshua Colwell

Laboratory for Atmospheric and Space Physics

University of Colorado

Campus Box 392

Boulder CO 80309-0392

Tel: 303-492-6805

Fax: 303-492-6946

[josh.colwell@lasp.colorado.edu](mailto:josh.colwell@lasp.colorado.edu)

**We present the results of the second flight of the Collisions Into Dust Experiment (COLLIDE-2), a space shuttle payload that performs six impact experiments into simulated planetary regolith at speeds between 1 cm/s and 100 cm/s. COLLIDE-2 flew on the STS-108 mission in December 2001 following an initial flight in April 1998 (Colwell and Taylor, 1999). The experiment was modified since the first flight to provide higher quality data and the impact parameters were varied. Spherical quartz projectiles of 1 cm radius were launched into quartz sand and JSC-1 lunar regolith simulant targets 2 cm deep. At impact speeds below ~20 cm/s the projectile embedded itself in the target material and did not rebound. Some ejecta were produced at ~10 cm/s. At speeds >25 cm/s the projectile rebounded and significant ejecta was produced. We present coefficients of restitution, ejecta velocities, and limits on ejecta masses. Ejecta velocities are typically less than 10% of the impact velocity, and the fraction of impact kinetic energy partitioned into ejecta kinetic energy is also less than 10%. Taken together with a proposed aerodynamic planetesimal growth mechanism (Wurm et al., 2001a), these results support planetesimal growth at impact speeds above the nominal observed threshold of about 20 cm/s.**

Key words: Planetary rings; planetesimals; experimental techniques; dust; collisions.

## I. Introduction

Observations of dust in the ring systems of each of the giant planets suggest a continuing supply of dust liberated from the surfaces of larger “parent” ring particles (e.g. Cuzzi and Burns, 1988; Colwell and Esposito, 1990a; de Pater et al., 1999).

Micrometeoroid bombardment of these parent objects provides one component of the dust source, but interparticle collisions may release a significant fraction as well (Colwell and Esposito 1990a, 1990b). Ring particles are likely coated with small particles reaccreted from the micrometeoroid ejecta (e.g. Cuzzi and Durisen 1990). Interparticle collision speeds in optically thick planetary rings have been collisionally damped, typically to speeds much less than 1 m/s. However, the small masses of ring particles make gravity negligible in determining the fate of dust on the surfaces of these particles, even in very slow collisions. In addition to being a source of dust for dust rings, the coating of small particles on the surfaces of larger ring particles acts as an efficient shock absorber that damps random velocities excited, for example, by gravitational perturbations from nearby or embedded moons.

Similar types of collisions likely played an important role in the early stages of planetesimal growth. These collisions likely occurred at relative velocities from a few 10's of m/s for very different-sized particles down to 10's of cm/sec for a 1 cm object colliding with a 10 cm object, either a laminar or turbulent nebula (Weidenschilling and Cuzzi 1993). Escape velocities from meter-sized particles are on the order of  $10^{-3}$  m/s, so collisions must be highly inelastic in order for growth to proceed. Dusty regolith covering particles may have helped to dissipate collisional energy, reducing the rate of

mass loss during collisions and promoting accretional growth of larger bodies. However, if the particles consist of unconsolidated dust, then even at low velocities these aggregates may fragment and net erosion rather than accretion could occur. Blum and Wurm (2000), Wurm and Blum (1998), Blum et al. (2000), and Poppe et al. (2000) have experimentally studied the collisional growth of aggregates of dust, and the sticking and rebound properties of individual dust particles at low speed impacts. Dominik and Tielens (1997) study the physics of dust coagulation and compaction and find that cm-sized aggregates can form in the solar nebula without significant compaction. Wurm et al. (2001a, 2001b) have looked at the growth and erosion of dust aggregates in the presence of nebular gas drag on grains. The latter showed that even if small particles are liberated in a collision, they may quickly become entrained in the gas of the protoplanetary nebula and returned to the surface of the larger object and reaccrete. The amount of ejecta produced in such collisions, and the velocities of the resulting ejecta, are poorly understood.

The effects of surface properties, including frost and dust, on the coefficient of restitution in low velocity collisions have been experimentally studied by Bridges et al. (1984), Hatzes et al. (1988), Supulver et al. (1995), and Dilley and Crawford (1996) using hard ice particles and pendulums to achieve impact velocities less than 1 cm/s, typical of planetary ring particle impact velocities (e.g. Esposito, 1993). Hatzes et al. (1988) used frosted ice impactors such as might be found in planetary rings, but there was no unconsolidated regolith and therefore no ejecta studies. Hartmann (1978) measured coefficient of restitution as a function of regolith thickness for normal impacts into granular material at several m/s impact speeds. Hartmann (1985) performed impact

experiments at speeds as low as 5.3 m/s into granular material and reported on the production of ejecta. Colwell and Taylor (1999; Paper 1 hereafter) reported on the first results from the microgravity experiment described here, which were the first to study ejecta production at speeds below 1 m/s. In this paper we describe the results from the second flight of the Collisions Into Dust Experiment (COLLIDE-2) and its implications for the early stages of planetesimal formation and dust production in planetary rings.

In the next section we describe the experimental procedure, and in section III we present results from the flight data. We conclude with a discussion of the implications of the results on planetary ring and protoplanetary disk dynamics.

## II. Experimental Procedure

In order to study low-velocity collisions into a dust-covered surface such as occur between small particles in space, a microgravity environment is necessary. COLLIDE first flew on the space shuttle as a Get Away Special (GAS) payload on STS-95 in April 1998 (Paper 1). The basic configuration of the experiment for the COLLIDE-2 flight is unchanged from that described in Paper 1. Here we summarize the experiment configuration and describe those changes to the experiment that were made to ensure proper functioning. A concurrent set of ground-based experiments has been performed for comparison with COLLIDE (Colwell and Mellon, 2002), and a series of reduced-gravity experiments on the NASA KC-135 reduced gravity aircraft is underway (Colwell et al., 2002).

COLLIDE-2 is a self-contained autonomous payload that was part of the MACH-1 Hitchhiker bridge on space shuttle Endeavour mission STS-108. The experiment performs six independent impacts at approximately normal incidence angle into a bed of

granular material. Each impact takes place in a self-contained and independent Impactor Box System (IBS). Each IBS consists of a spring-powered projectile launcher approximately 10 cm from the surface of a target of granular material that is held in place prior to the experiment by a sliding door. The impacts are recorded on two digital video tapes recorded by digital video camcorders inside the experiment. Illumination is provided by light emitting diodes in the IBS. The experiment container was evacuated and sealed prior to launch. The camcorders are in two sealed containers at 1 atmosphere of pressure to provide a normal operating environment.

A baroswitch on the exterior of the container turned on the experiment electronics within the first minute of the launch. The experiment program follows a 14-hour software timer before beginning execution of the experiment during a crew sleep period to minimize accelerations. Two data loggers were flown to provide verification of experiment operation and timing. A temperature data logger with four temperature sensors recorded increases in temperatures as voltage regulators turned on during execution of the experiment. A light-sensitive data logger was positioned to detect the lights inside IBS 3. This provided another indication of the timing of the experiment for correlation with telemetry on the space shuttle attitude control system which automatically fires thrusters on the orbiter to maintain attitude.

The orbiter launched at 22:19 UTC on December 5, 2001. The first experiment activity was a three-minute warm-up of each of the camcorders. This is a change from the first flight of COLLIDE to counter camera recording problems the first time the cameras were used. The sealed containers for the cameras were redesigned to prevent a recurrence of the leaks on the first flight. One camera container experienced partial leaking on

COLLIDE-2, however both cameras functioned properly. The ambient pressure in the experiment canister was less than  $1.3 \times 10^3$  Pa.

The temperature data indicate an experiment start time of 12:21:00 UTC on December 6, 2001. Comparison of the experiment impact times with data from the space shuttle orbiter's Reaction Control System firing times showed that no thruster firings occurred during the impacts. Video data also show no indications of any residual acceleration. Data were returned on the two digital videotapes and retrieved for analysis from the experiment in January 2002.

Two different target materials were used on COLLIDE-2: silica (quartz) sand and JSC-1 lunar regolith simulant. All targets had a depth of 2 cm over a solid Aluminum base. Both samples were sieved to a size distribution between 75 and 246  $\mu\text{m}$ . The silica particles are rounded in shape while the JSC-1 particles are angular (Figure 1). Average grain size for the silica particles is 220  $\mu\text{m}$ , while the average size for unsieved JSC-1 is about 100  $\mu\text{m}$ . These particles are significantly larger than the  $\sim$ micron-sized spheres used in dust aggregation and sticking experiments cited above, but are similar to those used in high-velocity impact experiments and COLLIDE-1. A study of the effects of particle size on impact outcome was not possible with the limited number of impact experiments on COLLIDE-2. JSC-1 is a glass-rich basaltic ash which has similar chemical composition, mineralogy, particle size distribution, and engineering properties to lunar mare regolith (McKay et al. 1994). The internal angle of friction of JSC-1 is 45 degrees, while for the silica sand it is 34 degrees. Although both of these numbers depend on the confining pressure, the difference reflects the rounder shape of the sand particles making them less able to sustain a steep slope. For the impact experiments described

here, this means that the particles in the sand targets are freer to roll across each other in response to an impact while JSC-1 particles behave more like interlocking gears.

Minimal filling of the target trays under 1 g corresponds to a relative density,  $D_r = 0$ , where relative density is defined by

$$D_r = \frac{e_{\max} - e}{e_{\max} - e_{\min}}. \quad (1)$$

A relative density of 1 corresponds to the density of the material achieved following vibration with a compressive force on the material. The material constants  $e_{\max}$  and  $e_{\min}$  are determined experimentally by measuring void ratios of the material following compression and vibration ( $e_{\min}$ ) and with no load applied ( $e_{\max}$ ). The void ratio,  $e$ , is defined by

$$e = \frac{G_s \rho_w}{\rho_d} - 1 \quad (2)$$

where  $G_s$  is the specific gravity of the material (density relative to water),  $\rho_w$  is the density of water ( $1.0 \text{ g/cm}^3$ ), and  $\rho_d$  is the bulk density of the sample. The void ratio is related to the porosity,  $n$ , by  $n=e/(1+e)$ . For JSC-1,  $G_s=2.9$ ,  $e_{\max}=1.028$ , and  $e_{\min}=0.585$ . For the silica particles,  $G_s=2.65$ ,  $e_{\max}=0.805$ , and  $e_{\min}=0.486$  (Batiste, 2001). On COLLIDE-2 each IBS was filled as closely as possible to a relative density of 0, by not using any shaking or compression of the samples, and not overfilling the target tray volumes. The main uncertainty in this value is in the actual free volume available to the target material because of the presence of flexible materials within the target tray designed to prevent jamming of the target tray door mechanism. We estimate this uncertainty to be about  $1 \text{ cm}^3$ .

The two minutes of extreme vibration during launch of the shuttle raises the possibility of settling and an increase of the relative density. We tested the response of our samples to vibration on the ground and found that there was no significant compression of the quartz sand due to vibration alone, and removing the particles small than 75  $\mu\text{m}$  significantly reduced the settling of the JSC-1 seen in the first flight of COLLIDE. There was no settling visible in the data for any of the target samples. Accelerations due to launch vibration are significantly greater than the acceleration of the shuttle itself ( $<3\text{g}$ ). The relatively small masses of the target samples ( $\sim 300\text{ g}$ ) are too low for fracturing of grains or significant compression with that acceleration.

Another possible consequence of the launch vibration is leaking of the target grains into the door mechanism. Two of the six IBS target tray doors jammed on the first flight (paper 1), so a new system of particle barriers was designed for COLLIDE-2. This involved a vacuum grease seal along the inside boundary of the target tray door which reduced the volume of the trays by about  $1\text{ cm}^3$  compared to a total volume of  $229\text{ cm}^3$ . The uncertainty in the target mass is less than 1 g out of approximately 300 g, so the uncertainty in the bulk density is less than 1 per cent. Each target tray door functioned properly on COLLIDE-2. The bulk densities, void ratios, and porosities for each IBS measured prior to flight are included in Table 1 along with observed impact parameters. For comparison, the porosity of the top 1 cm of lunar regolith is 0.59, corresponding to a bulk density of  $1.4\text{ g/cm}^3$ , based on interpretation of microwave observations during a lunar eclipse (Sandor and Clancy 1995).

Table 1: Experimental Parameters

IBS	1	2	3	4	5	6
Parameter						
Measured Impact Speed (cm/s)	110±10	3.60±0.1	1.29±0.01	81±10	12.2±0.1	28±2
Projectile mass (g)	10.71	9.64	10.29	8.66	8.98	10.62
Target material	Quartz Sand	Quartz Sand	Quartz Sand	Quartz Sand	JSC-1	Quartz Sand
Target bulk density (g/cm <sup>3</sup> )	1.49	1.53	1.50	1.52	1.25	1.49
Target void ratio	0.78	0.73	0.77	0.74	1.32	0.78
Target porosity	0.44	0.42	0.43	0.43	0.57	0.44
Target Relative Density	0.07	0.23	0.12	0.18	N/M	0.09

The density of the projectiles is 2.65 g/cm<sup>3</sup>. All impactors are approximately 2 cm in diameter. The depth of the target material is 2 cm for all targets. Both target materials were sieved to particle size ranges of 75-250 microns. The void ratio for the JSC-1 target exceeds the nominal maximum value for unsieved JSC-1 (1.028) because all particles smaller than 75 microns were removed. These small particles would normally fill void spaces leading to a lower porosity. For this reason, the relative density of the JSC-1 target is not measured (N/M). Uncertainties in void ratio, porosity, and relative density are estimated to be less than 1 per cent. Uncertainties in impact speed are based on uncertainty in measuring impactor position. This is controlled by pixel size at the slowest speeds and image smear at the fastest speeds.

The geometry of the impacts, the camera views, and the sequence of operation of the experiment are the same as described in paper 1. The only change to the experiment sequence was the addition of camera warm-up periods prior to running the experiment. The experiment was powered by its internal set of 24 D-cell alkaline batteries in three redundant parallel stacks of 8 cells.

### III. Experimental Results

#### A. Overview

Except for the data logger temperature and light sensor engineering data mentioned above, all COLLIDE-2 data are contained on two digital videotapes recorded by the onboard camcorders. Because each camcorder has a fixed orientation and views three IBSs at the opposite end of the experiment simultaneously, each IBS only fills

about one-sixth of the camcorder field of view. The data are therefore at low spatial resolution, and the target silica and JSC-1 grains are sub-pixel. An example frame from IBS 1 is shown in Figure 2 with a schematic that identifies elements in the scene. The objectives for COLLIDE-2 were (1) to identify the transition between impacts that produce significant ejecta (erosional impacts) and those that do not produce ejecta (accretional impacts), (2) to measure coefficients of restitution for impacts into regolith at low impact velocities, (3) to measure the velocity of ejecta produced in the impact, and (4) to constrain the ejecta mass. The range of impact velocities was chosen to span the likely transition regime based on results from COLLIDE and ground-based impact experiments at 1 m/s and higher speeds.

All six IBSs operated nominally, and Table 2 summarizes the outcomes of each impact experiment. The experiment successfully met the primary objective of bracketing the transition between erosional (net mass loss from target) and accretional (net mass gain by target) impacts which, for the materials and impactor sizes studied here, occurs at an impact speed of about 10-20 cm/s. We were also able to measure normal coefficients of restitution,  $\epsilon_n = v_n/v_i$ , where  $v_n$  is the normal component of the rebound velocity, and  $v_i$  is the normal component of the impact velocity. Tangential coefficients of restitution were not directly measured, however, because in those impacts where the projectile rebounded, fiduciary marks on the projectiles were not visible for tracking rotation due to interference from ejecta particles. The projectile launcher design can lead to a rotation of the projectile prior to impact (paper 1), and the projectiles that rebounded did so at an angle to the surface, implying non-zero rotation prior to impact. Assuming that the projectiles rolled through the launcher tube without slipping provides an upper limit to

the pre-impact rotation rate from the velocity and the projectile size. Assuming zero rotation of the projectile after impact leads to lower limits on the tangential coefficients of restitution (Table 2).

In two of the six impact experiments no ejecta was produced. In three of the remaining four the ejecta curtain was optically thick and because the particles are sub-pixel scale, only a gross characterization of ejecta velocities was possible. In the final impact, individual ejecta particles were tracked providing a direct measure of ejecta velocities. The details of the ejecta velocity analysis are below. Ejecta masses cannot be measured directly because some target particles are released from the target after the impact by the closing of the target tray door. In addition, static charging of the target surface prior to the impact by the opening of the target tray door resulted in some particles leaving the surface prior to the impact. An upper limit on ejecta mass can be placed from the amount of target material recovered from the target tray, but more meaningful estimates may be arrived at from comparison of the video data with video data from ground-based experiments for which ejecta masses are measured by other methods (Colwell and Mellon, 2002). This is the basis of the constraints on ejecta mass below.

Projectile velocities before and after impact were obtained by measuring the change in position of the projectile from one frame to the next of the digital videotape. The frame rate is 29.97 frames per second, so the uncertainty in speeds is larger at higher speeds. Projectile trajectories were tracked manually using Spotlight tracking software provided by NASA Glenn Research Center. Velocities are determined from least-squares linear fits to the tracking data. No accelerations were detectable.

Table 2: Experiment Summary

IBS	Impact Speed (cm/s)		Rebound Speed (cm/s)		$\epsilon_n$	$\epsilon_t$	Crater Diameter (cm)	Maximum Ejecta Velocity (cm/s)
	X	Y	X	Y				
1	0±2	110±10	0.85	1.10	0.01	$7.7 \times 10^{-3}$	6±2	10±1
2	0.01±0.01	3.62±0.04	0	0	0	0	0	0
3	0.14±0.04	1.29±0.01	0	0	0	0	0	0
4	0±2	81±10	0.67	1.2	0.015	$8.3 \times 10^{-3}$	N/M	16±1
5	0.12±0.06	12.15±0.1	0	0	0	0	0	1.5±0.2
6	2.4±1	24.9±2	0.32	0.50	0.02	$1.1 \times 10^{-2}$	4±2	3±1

Notes: The coordinate system for each IBS is defined so that the Y axis is normal to the target surface. Speed uncertainties are the higher of the formal 1-sigma uncertainty in the fit to the trajectory data or the uncertainty introduced by smear in the image.  $\epsilon_n$  is the ratio of the normal component of the rebound velocity to the normal component of the impact velocity.  $\epsilon_t$  is a lower limit on the tangential coefficient of restitution assuming zero post-impact rotation. Movement out of the X-Y plane was not measured. N/M = Not measured. Crater diameters of 0 represent impacts where the impactor embedded itself in the target without creating a detectable larger displacement of target material. See text for details on ejecta velocities.

### B. Coefficient of Restitution.

Bridges et al. (1984) and Hatzes et al. (1988) performed impact experiments with frosted and unfrosted ice spheres at velocities less than 1 cm/s and found a relationship between coefficient of restitution and impact speed. Dilley (1993) examined the functional dependence of the coefficient of restitution on particle size and mass, and Dilley and Crawford (1996) performed ice impact experiments at 1 cm/s with different impactor masses. Supulver et al. (1995) performed normal and glancing collisions of ice spheres with an ice brick and measured normal and tangential coefficients of restitution. In paper 1 we found coefficients of restitution of about 0.02-0.03 for impacts into compacted JSC-1 at 15, 17, and 90 cm/s (paper 1). With the less compacted targets in COLLIDE-2 the normal coefficients of restitution are even lower, with no rebound observed at impact speeds of 12 cm/s and below.

### *C. Ejecta Velocities.*

The impact in IBS 5 into JSC-1 at 12 cm/s produced a sparse ejecta curtain of slow particles that could be individually tracked. These particles were tracked in the same way that the projectiles were tracked for impact and rebound velocities, though some ejecta particles were tracked using an automatic tracking feature of the Spotlight tracking software. Because the particles are sub-pixel, their brightnesses vary, and they are occasionally lost from view when passing in front of light markings on the background. Particles were therefore only tracked over parts of their trajectories, and manual tracking was used when the automatic tracking could not lock onto particles consistently. Figure 3 shows the trajectories of 26 particles from the impact in IBS 5. We estimate that this represents approximately one half to one quarter of all the ejecta particles and clumps released in the impact. Full sampling of ejecta trajectories was not possible because some particles are too faint to be reliably tracked against the background, either because of small size, a path that lay consistently in front of one of the bright background markings, or a path in front of or behind the projectile. 37 particles were tracked and later analysis showed that only 26 of these were unique. The last 8 particles selected for tracking were duplicates of previous particles, so we believe all particles that could be reliably tracked have been tracked.

Figure 4 shows the X and Y components of the measured ejecta speeds,  $V_X$  and  $V_Y$ . The component of the velocity out of the camera plane was not measured. The relative lack of particles with small  $V_Y$  is a selection effect: the impact was in the Y direction, and particles with small  $V_Y$  were too close to the target surface, where the background was bright and cluttered by loose particles, for tracking. 24 of the 26 particles

had  $V_X < V_Y$ , consistent with a simple ejecta cone model with a cone opening angle (angle between the target normal and the ejecta velocity vector) of  $\theta = 45$  degrees or less, where smaller  $V_X$  corresponds to larger  $V_Z$ , (component of velocity normal to the image plane) which could not be measured. The distribution of ejecta velocities measured from the X and Y components is shown in Figure 5; in this simple ejecta cone model the total ejecta velocity is simply  $V_Y / \cos\theta$ . That is, if all the ejecta are ejected at a single ejecta cone angle,  $\theta$ , then  $V_Y / V = \cos\theta$  is the same for all particles, and  $V_X$  and  $V_Z$  differ depending on the azimuthal angle around the cone axis. Making this assumption results in an ejecta velocity distribution similar to that for the X and Y components alone: most particles' velocities are between 0.3 and 0.8 cm/s.

In the three remaining experiments in which ejecta was produced on impact, we have measured the velocities of the ejecta curtains but not individual particles. The schematic in Figure 2 shows five components of the ejecta curtain for IBS 1. For this impact at 110 cm/s, the ejecta boundary velocities indicate a maximum ejecta velocity of  $\sim 10 \pm 1$  cm/s, and the velocities of each measured boundary are given in Figure 2. The speed of the center of the ejecta curtain ( $V_A = 7.2 \pm 0.2$  cm/s) is the projected speed in the image plane, while the speeds along the diagonal tracks ( $V_B$  and  $V_C$ ) have no projection effect. A cone opening angle of  $\theta = 45$  degrees corresponds to a full speed at the center of the ejecta curtain of  $V = V_A / \cos\theta = 10.2$  cm/s, compared with the values for  $V_B$  and  $V_C$  of 8.7 and 11.1 cm/s, respectively.

The impact in IBS 4 at 81 cm/s resulted in slightly higher maximum ejecta velocities of 16 cm/s. That impact produced discrete rays of ejecta in the curtain. The trajectories of tracked points on the ejecta curtain along with the velocities (in the plane

of the image) are shown in Figure 6. The target in IBS 4 was slightly denser than the target in IBS 1, but there is insufficient data to conclusively link that to the higher ejecta speeds. The impact in IBS 6 at 25 cm/s produced a cloud of ejecta that was too dense for individual particle tracking but not as symmetric or with as clearly identifiable ejecta curtain boundaries as in IBS 1 and IBS 4. The projectile struck the surface at a slightly oblique angle (Table 2) resulting in an asymmetric distribution of ejecta (Figure 7). We tracked seven points along the ejecta boundary using both manual and automatic tracking resulting in ejecta velocities of 1.5 to 3.5 cm/s. Roughly, the results from the four impacts that produced measurable ejecta indicate a maximum ejecta speed of 10-15% of the impactor speed.

#### *D. Ejecta Mass*

Direct measurement of the ejecta mass could only be achieved by comparing the target mass in the target tray before and after the flight. Some particles were lifted off the target surface prior to impact by electrostatic forces, and the target tray doors did not completely reseal the target tray after impact. Therefore the measured amount of remaining target material only provides a rough upper limit on the ejecta mass. Comparisons with the video data show that even in the case where clearly no impact ejecta were produced the amount of material that left the target tray due to these two effects was over 40 g.

One approach to get a firm upper limit on the ejecta mass is to assume that all the kinetic energy of the impactor went into kinetic energy of the ejecta. Taking the extreme assumption that all ejecta travel at the highest ejecta speeds measured, this provides upper limits on the ejecta mass between 110 and 530 g for the various impacts, which is clearly

far higher than the actual ejecta masses. For the two fastest impacts the results indicate that at most 15% of the available kinetic energy was partitioned into ejecta kinetic energy, again with the assumption that all ejecta travels at the highest observed speeds. By adjusting the recovered target masses for the estimated pre-impact loss of ~40 g, and accounting for ejecta moving at less than the highest ejecta velocities (e.g. Figures 2, 7), we conservatively estimate that the actual ejecta kinetic energy fraction is lower by at least a factor of 2.

While the JSC-1 target had a significantly higher porosity than the quartz sand targets, the more angular nature of the grains may have reduced the amount of flow in the target in response to the impact and therefore reduced the amount of ejecta liberated from the surface. Ground-based experiments at 1-2.3 m/s have shown that the size distribution and angularity of the target grains plays an important role in the amount of ejecta produced (Colwell and Mellon 2002).

The impact into JSC-1 produced an optically thin ejecta cloud in which all ejected particles could be observed (Figure 5). The low resolution of the video does not allow us to resolve each particle or clump of particles, however. We estimate 50-100 clumps or particles. If each clump is a single grain of JSC-1 at the minimum particle size of 75 microns, then the ejecta mass is  $\sim 3 \times 10^{-5}$  g. This must be regarded as an extreme lower limit. If, on the other hand, the clumps are in fact agglomerates of several grains, with close packing and the interparticle voids filled with small particles, then based on the resolution of the video (~600 microns/pixel) the mass of each clump could be as much as ~500 times higher, and the upper limit on the ejecta mass for this impact is ~0.03 g.

## IV. Conclusions and Discussion

The main results of the COLLIDE-1 and COLLIDE-2 experiments are:

- 1 cm radius particles embed themselves in loose, deep, granular beds (COLLIDE-2) at impact speeds up to at least 12 cm/s. Impacts at 25 cm/s and higher result in rebound, and impacts at 15 cm/s into a dense, deep, granular bed (COLLIDE-1) also result in rebound, with normal coefficients of restitution of  $\sim 0.02$ .
- No ejecta was produced at impacts of 4 cm/s and slower into a loose granular bed, ejecta mass at 12 cm/s is  $< 0.03$  g, and none was produced at 15 cm/s into a dense granular bed. Ejecta masses at impacts of 25 cm/s and higher into loose quartz sand were  $> 10$  g.
- Maximum characteristic ejecta velocities for impacts between 12 cm/s and 108 cm/s are  $\sim 0.1$  of the impact velocity.
- The total fraction of impactor kinetic energy partitioned into ejecta kinetic energy is less than 0.1.

The impact experiments described here are in the same velocity and gravity regime as many impacts in planetary rings and protoplanetary disk environments. However, they cannot be considered as direct simulations of those collisions because we use different materials and we do not collide two dust-coated, free-floating, irregular, simulated ring particles. Nevertheless, with the results from two flights of COLLIDE and our ongoing ground-based and airplane-based experiments, we can begin to draw some general conclusions about the behavior of small particles in microgravity collisions and the implications for both planetesimal growth and planetary ring dynamics. Reduced

gravity airplane experiments will be described in detail elsewhere, but preliminary analysis of the first experiments shows results consistent with those reported here.

Colwell and Esposito (1990a, 1990b) modeled the production of dust in the ring systems of Uranus and Neptune from a combination of micrometeoroid bombardment of macroscopic ring particles and moonlets and collisions between ring particles. For dust production from ring particles their nominal model produced roughly two thirds of the observed dust from interparticle collisions and one third from micrometeoroid ejecta (Colwell and Esposito, 1990a (CE90), their Table II). In the absence of appropriate experimental data they used the same model for ejecta mass for high velocity and low velocity collisions. This high velocity impact model predicts  $10^{-3}$  g of ejecta for impacts like those in IBSs 1 and 4 on COLLIDE-2, and less for the lower velocity impacts but with no lower cutoff. The collisions in COLLIDE-2 produced far more ejecta at 100 cm/s than the CE90 model predicts, however that model also predicts significant ejecta at 10 cm/s if the masses of the colliding objects are large. This discrepancy is not surprising given the very different nature of hypervelocity impacts, in which a shock wave propagates through the target and ejecta is produced in the far field of the impact, from the low velocity impact studied here in which ejecta is produced in the near field of the impact through interparticle collisions. COLLIDE-2 results and our ground-based experiments (Colwell and Mellon 2002) confirm that new scaling models are needed for this impact regime.

The COLLIDE-2 data reported here only show a variation in impact speed, so further experiments are needed to learn the effects of impactor size and mass. Extrapolating from the cm-sized impactors in COLLIDE-2 to the Uranus moonlet belt

size regime (100 m) suggests that collision velocities are either slightly higher than the 10 cm/s used by CE90 or that most of the dust is generated by micrometeoroid impacts rather than interparticle collisions. The latter can be accomplished by making the size distribution of the moonlets steeper or the optical depth higher so that more surface area is exposed to the micrometeoroids. The observational constraints are not strong enough to rule out either hypothesis, and the extrapolation of COLLIDE-2 results to much larger impactors must be considered speculative until more data at different sizes are collected.

Experimental studies of the collisional accretion in the early stages of planetesimal growth have shown that micron-sized spherical grains can stick to hard surfaces at impact speeds of 1-10 m/s with sticking possible at higher speeds for irregularly shaped particles (Poppe et al., 2000). Entrainment of rebounding dust can result in net growth at collision speeds of  $\sim 10$  m/s (Wurm et al., 2001b). Our experiments use significantly larger particles (mean particle size of 150  $\mu\text{m}$  compared to  $\sim 1$   $\mu\text{m}$  for the aggregation experiments), and consequently surface forces such as the van der Waals force are less effective. Particle sticking from electrostatic dipole charge distribution (Marshall 1998) may be important in suppressing ejecta at the lower impact speeds. We observe a threshold velocity of about 20 cm/s between erosive and sticking impacts (ejecta mass  $>$  impactor mass and impactor rebound at 25 cm/s, and ejecta mass  $<$  impactor mass ejecta with no rebound at 12 cm/s). This is far lower than what might be inferred from the amount of ejecta produced in ground-based impact experiments (e.g. Hartmann 1985, Weidenschilling and Davis, 1988) which suggest a threshold of about 10 m/s.

The ejecta velocities are low enough, however, that the aerodynamic growth mechanism of Wurm et al. (2001b) could make even the 1 m/s impacts in COLLIDE-2 lead to growth rather than erosion. In this model, small particles liberated in an impact are returned to the target surface after becoming entrained in the nebular gas. This mechanism works as long as the ejecta are small enough to allow rapid coupling to the gas and the growing planetesimal is large enough to be decoupled from it. The Wurm et al. experiments used micron-sized particles, compared to the ~100 micron particles in COLLIDE-2. The Wurm et al. mechanism leads to accretion of small particles at impacts as high as several m/s. If our observed ratio of ejecta velocity/impact velocity  $\sim 1/10$  holds for impacts into smaller particles, then coupled with the results of Wurm et al. accretion may occur for impacts at  $\sim 10$  times higher speeds if the impactor is an aggregate that either sticks or breaks into its constituent parts on impact. Blum and Wurm (2000) found that impacting agglomerates are broken apart at impact speeds above a few m/s. Further experiments are planned and underway to investigate the effects of varying target size distribution and impactor size (e.g. Colwell and Mellon 2002, Colwell et al. 2002).

We found that our 2-cm impactors rebounded at 25 cm/s and stuck at 12 cm/s, while on the first flight of COLLIDE impactors at 17 cm/s into denser targets also rebounded. Although the coefficients of restitution are low (1-2%), these rebound velocities are still above the negligible gravitational escape velocity of a 1 meter or even 10 meter planetesimal (i.e., 1-10 mm/s) for impacts at speeds greater than 1 m/s. At larger sizes, however, the weak gravity of the planetesimal may be enough to turn around impactors that rebound slowly off a regolith-covered surface. If growth to these sizes

involves collisions between aggregates, then the impactor might break into smaller particles which are subject to the aerodynamic growth mechanism rather than rebounding as a single object. Impact experiments with aggregates suggest that at sizes larger than a few cm the aggregates begin to be compacted by collisions (Blum and Wurm, 2000).

The results of Blum and Wurm (2000) suggest that the aggregates do not restructure or fragment in these slow collisions ( $< \text{few m/s}$ ). Our results show a 20 cm/s maximum impact velocity for planetesimal growth to occur in the meter size range for impacts involving solid macroscopic particles. We plan further experiments to study impacts of dust aggregates, rather than monolithic impactors, into regolith which will show how the aggregate nature of the impactor affects the production of ejecta and dissipation of impactor kinetic energy. There can be a broad range of collision velocities in the presence of the nebular gas, depending on the size ratio of the colliding particles (e.g., Weidenschilling and Cuzzi, 1993). Collision speeds as low as our threshold value of  $\sim 20$  cm/s require particles either very similar in size, or no larger than a few cm. Gravitational stirring will excite the random velocities to about the escape velocity of the largest particles in the system. This is a radius of  $\sim 200$  m for a velocity of 20 cm/s. Once objects get larger than that, the gravity of the larger planetesimals will move the transition velocity between erosion and accretion to higher values because of the low rebound ( $\sim 1$  per cent) and ejecta ( $\sim 10$  per cent) velocities.

Acknowledgments: This research was supported by NASA. Technical support from NASA's Shuttle Small Payloads Program office, Glenn Research Center, Brian Motil, Monica Hoffmann, and the Kennedy Space Center is gratefully acknowledged. This

paper benefited from discussions with Susan Batiste, Larry Esposito, Mihály Horányi, Glen Stewart, Stein Sture, and Gerhard Wurm, and from detailed reviews by Jürgen Blum and an anonymous referee.

## REFERENCES

- Barge, P. and R. Pellat 1991. Mass spectrum and velocity dispersions during planetesimal accumulation. *Icarus* **93**, 270-287.
- Batiste, S. N. 2001. An investigation of deformations in granular materials using computed tomography. *Ph.D. Dissertation*. University of Colorado, Boulder.
- Blum, J., and 26 colleagues 2000. Growth and form of planetary seedlings: Results from a microgravity aggregation experiment. *Phys. Rev. Lett.* **85**, 2426-2429.
- Blum, J., and G. Wurm 2000. Experiments on sticking, restructuring, and fragmentation of preplanetary dust aggregates. *Icarus* **143**, 138-146.
- Bridges, F. G, A. P. Hatzes, and D. N. C. Lin 1984. Structure, stability, and evolution of Saturn's rings. *Nature* **309**, 333-335.
- Colwell, J. E., and L. W. Esposito 1990a. A numerical model of the Uranian dust rings. *Icarus* **86**, 530-560.
- Colwell, J. E., and L. W. Esposito 1990b. A model of dust production in the Neptune ring system. *Geophys. Res. Lett.* **17**, 1741-1744.
- Colwell, J. E., and M. Taylor 1999. Low Velocity Microgravity Impact Experiments into Simulated Regolith. *Icarus* **138**, 241-249.
- Colwell, J. E., and M. Mellon 2002. Experimental Studies of Collisions in Planetary Rings and Protoplanetary Disks, 33<sup>rd</sup> Lunar and Planetary Science Conference, Mar. 11-15, Houston TX (Abs. #1757).

- Colwell, J. E., S. Sture, A. Lemos 2002. Microgravity Impact Experiments: The PRIME Campaign on the NASA KC-135. 6<sup>th</sup> Microgravity Fluid Physics and Transport Phenomena Conference, Aug. 14-16, Cleveland OH.
- Cuzzi, J. N., and J. A. Burns 1988. Charged particle depletion surrounding Saturn's F ring: Evidence for a moonlet belt? *Icarus* **74**, 284-324.
- Cuzzi, J. N., and R. H. Durisen 1990. Bombardment of planetary rings by meteoroids: General formulation and effects of oort cloud projectiles. *Icarus* **84**, 447-466.
- De Pater, I., M. R. Showalter, J. A. Burns, P. D. Nicholson, M. C. Liu, D. P. Hamilton, and J. R. Graham 1999. Keck Infrared Observations of Jupiter's Ring System near Earth's 1997 Ring Plane Crossing. *Icarus* **138**, 214-223.
- Dilley, J. P. 1993. Energy loss in collisions of icy spheres: Loss mechanism and size-mass dependence. *Icarus* **105**, 225-234.
- Dilley, J. P., and D. Crawford 1996. Mass dependence of energy loss in collisions of icy spheres: An experimental study. *J. Geophys. Res.* **101**, 9267-9270.
- Dominik, C., and A. G. G. M. Tielens 1997. The physics of dust coagulation and the structure of dust aggregates in space. *Astrophys. J.* **480**, 647-673.
- Esposito, L. W. 1993. Understanding Planetary Rings. *Annu. Rev. Earth Planet. Sci.* **21**, 487-523.
- Hartmann, W. K. 1978. Planet formation: Mechanism of early growth. *Icarus* **33**, 50-62.
- Hartmann, W. K. 1985. Impact experiments. 1. Ejecta velocity distributions and related results from regolith targets. *Icarus* **63**, 69-98.
- Hatzes, A. P., F. G. Bridges, and D. N. C. Lin 1988. Collisional properties of ice spheres at low impact velocities. *Mon. Not. R. Astr. Soc.* **231**, 1091-1115.

- Marshall, J. R. 1998. "Coulombic Viscosity" in granular materials: Planetary and astrophysical implications. 29<sup>th</sup> Lunar and Planetary Science Conference, Houston TX.
- McKay, D. S., J. L. Carter, W. W. Boles, C. C. Allen, and J.H. Allton 1994. JSC-1: A new lunar soil simulant. *In Engineering, Construction, and Operations in Space IV*, American Society of Civil Engineers, 857-866.
- Poppe, T., J. Blum, and T. Henning 2000. Analogous experiments on the stickiness of micron-sized preplanetary dust. *Astrophys. J.* **553**, 454-471.
- Sandor, B. J., and R. T. Clancy 1995. Microwave observations and modeling of a lunar eclipse. *Icarus* **115**, 387-398.
- Supulver, K. D., F. G. Bridges, and D. N. C. Lin 1995. The coefficient of restitution of ice particles in glancing collisions: Experimental results for unfrosted surfaces. *Icarus* **113**, 188-199.
- Weidenschilling, S. J., and D. R. Davis 1988. Dust to dust: Low-Velocity impacts of fragile projectiles. 19<sup>th</sup> Lunar and Planetary Science Conference, Houston TX.
- Weidenschilling, S. J., and J. N. Cuzzi 1993. Formation of planetesimals in the solar nebula. In *Protostars and Planets III* (E. H. Levy, J. I. Lunine, Eds.), pp. 1031-1060, Univ. Arizona Press, Tucson.
- Wurm, G., and J. Blum 1998. Experiments on preplanetary dust aggregation. *Icarus* **132**, 125-136.
- Wurm, G., J. Blum, and J. E. Colwell 2001a. A new mechanism relevant to the formation of planetesimals in the solar nebula. *Icarus* **151**, 318-321.

Wurm, G., J. Blum, and J. E. Colwell 2001b. Aerodynamical Sticking of Dust  
Aggregates. *Phys. Rev. E*, **64**, #046301.

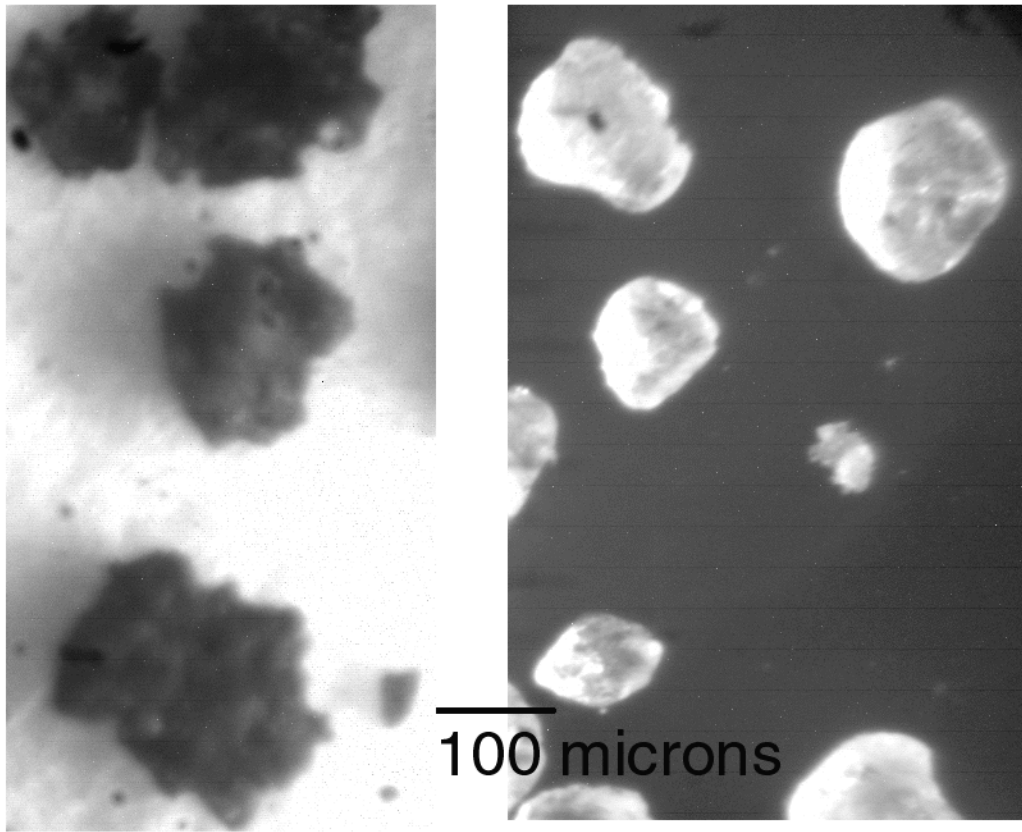


Figure 1: Photographs of JSC-1 particles (left) and silica quartz sand (right) used as target materials in COLLIDE-2. The scale bar is 100 microns long.

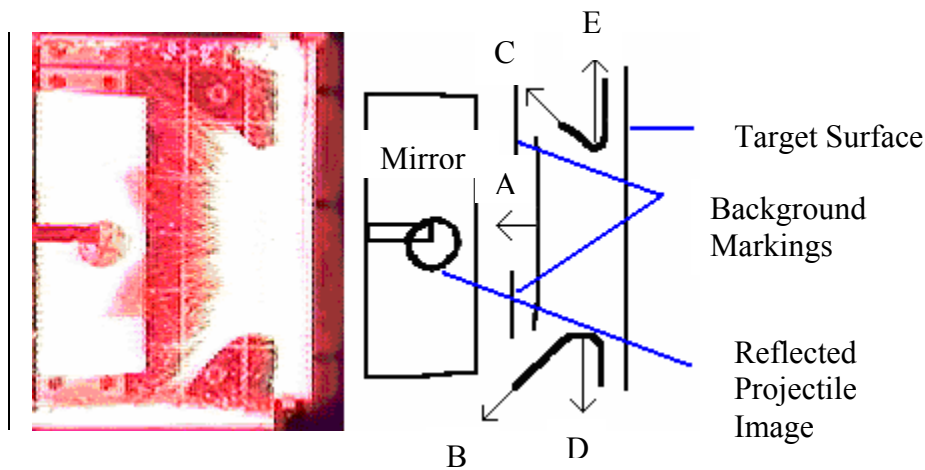


Figure 2: Still frame from IBS 1 0.3 seconds after impact and schematic of the image frame. The target surface is vertical at right, and the projectile motion was horizontally from the left. An image of the projectile on the target surface is visible in the mirror at left. Lettered arrows indicate the points on the ejecta curtain that were tracked for this IBS, and blue lines identify some of the elements in the image. Similar points on the ejecta curtains of IBS 4 and IBS 6 were tracked. Measured velocities of each point:  $V_A = 7.2 \pm 0.2$  cm/s;  $V_B = 8.7 \pm 0.3$  cm/s;  $V_C = 11.1 \pm 0.4$  cm/s;  $V_D = 1.7 \pm 0.1$  cm/s;  $V_E = 2.7 \pm 0.1$  cm/s.

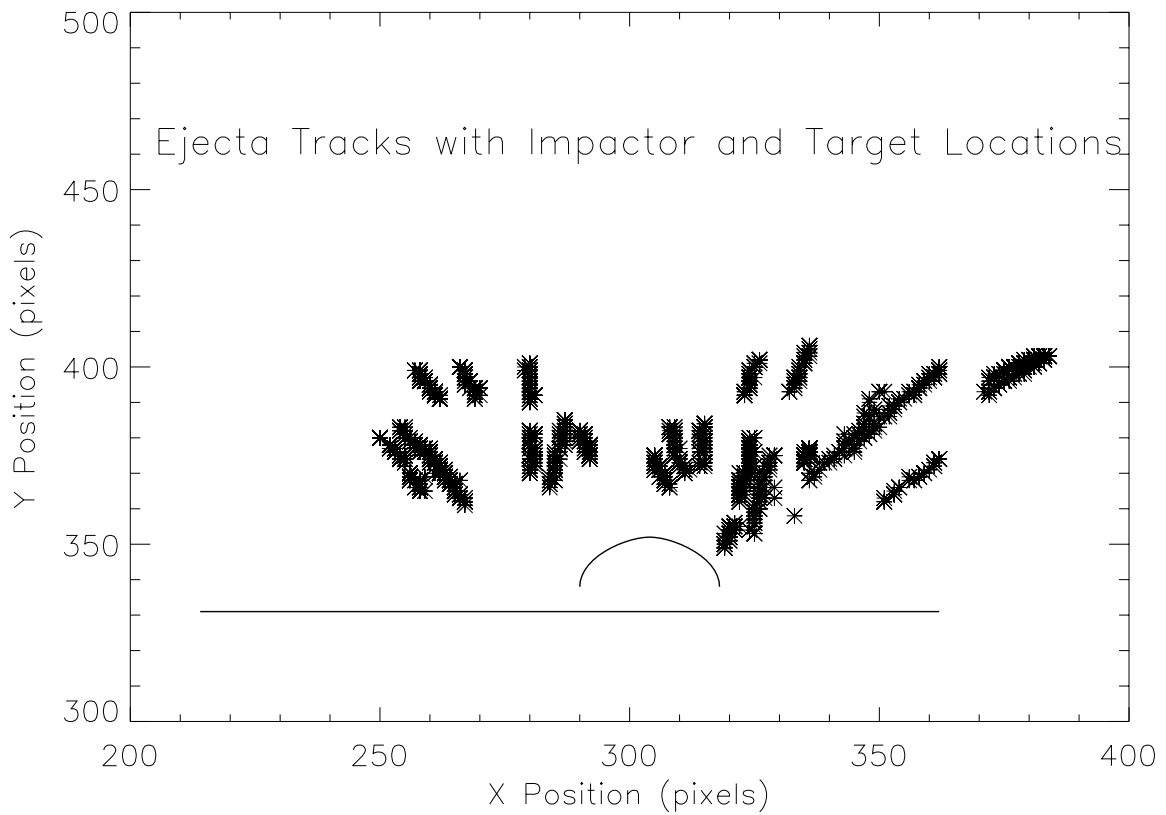
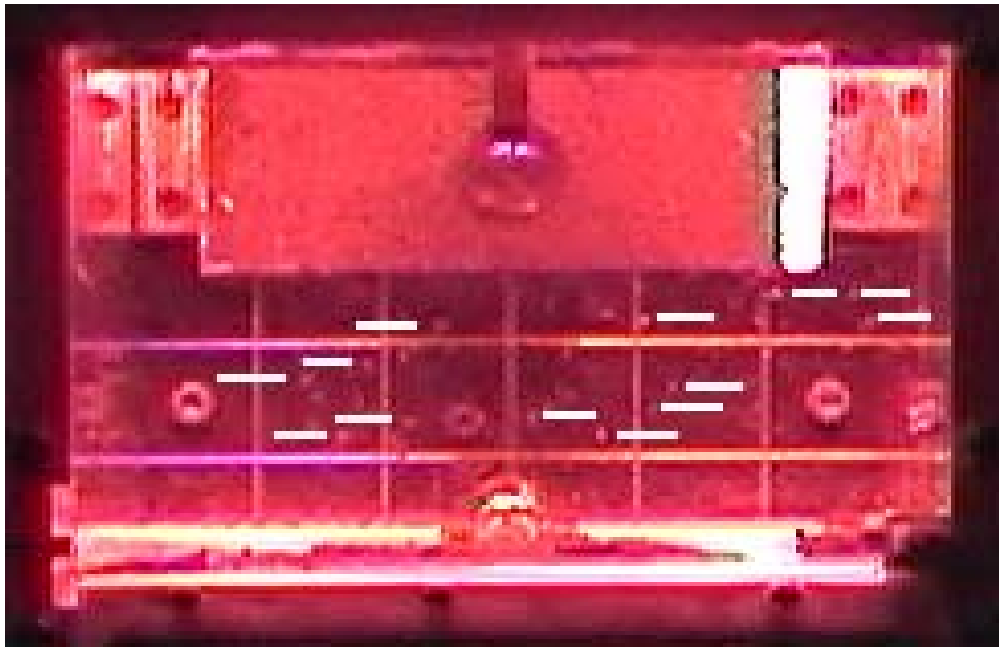


Figure 3: A frame from the impact in IBS 5 (top) showing individual particles and clumps of ejecta (some are marked by the white lines). The bottom frame shows a

superposition of the trajectories of individual particles and clumps of particles ejected in the impact in IBS 5, with the target surface and post-impact projectile position indicated.

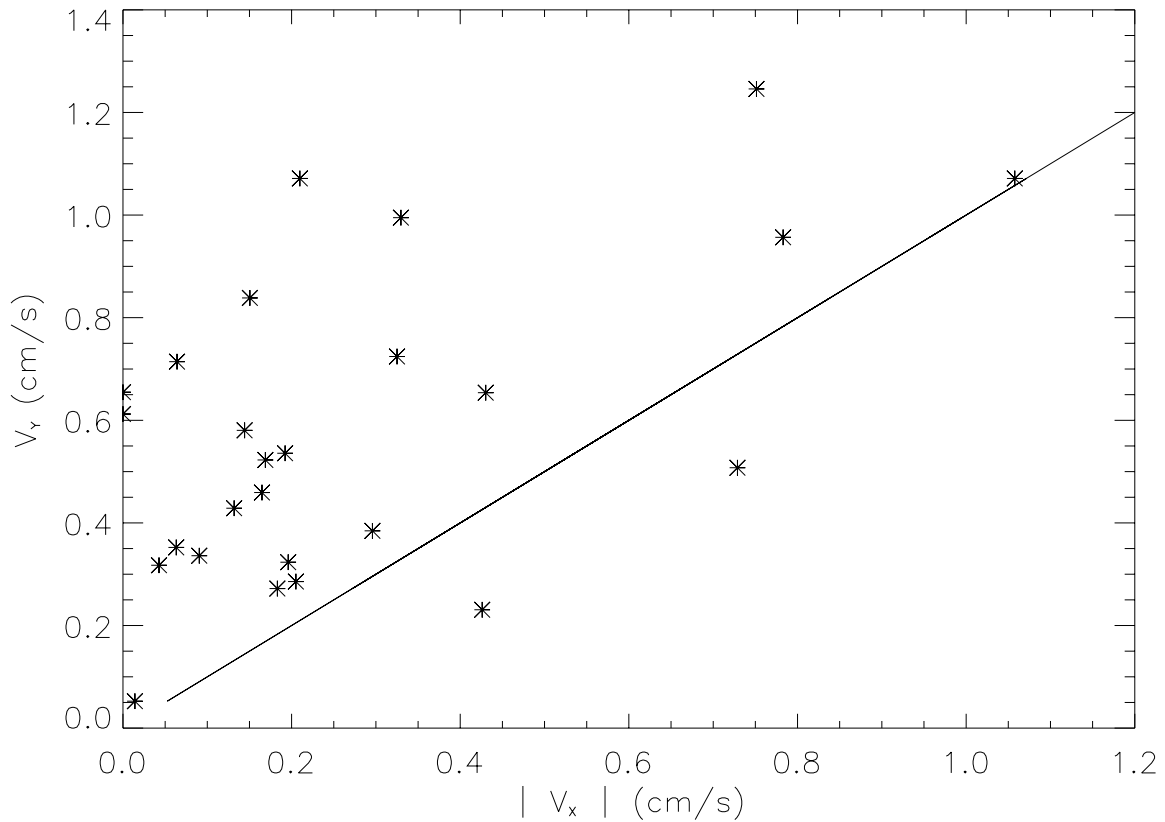


Figure 4: Scatter plot of measured  $V_X$  and  $V_Y$  components of ejecta from the IBS 5 impact. Measurement error of these slow velocities is conservatively estimated at less than 10 per cent. Only the two particles below the line had  $V_X > V_Y$ . The rest are consistent with an ejecta cone opening angle of 45 degrees (or less, measured from the surface normal).

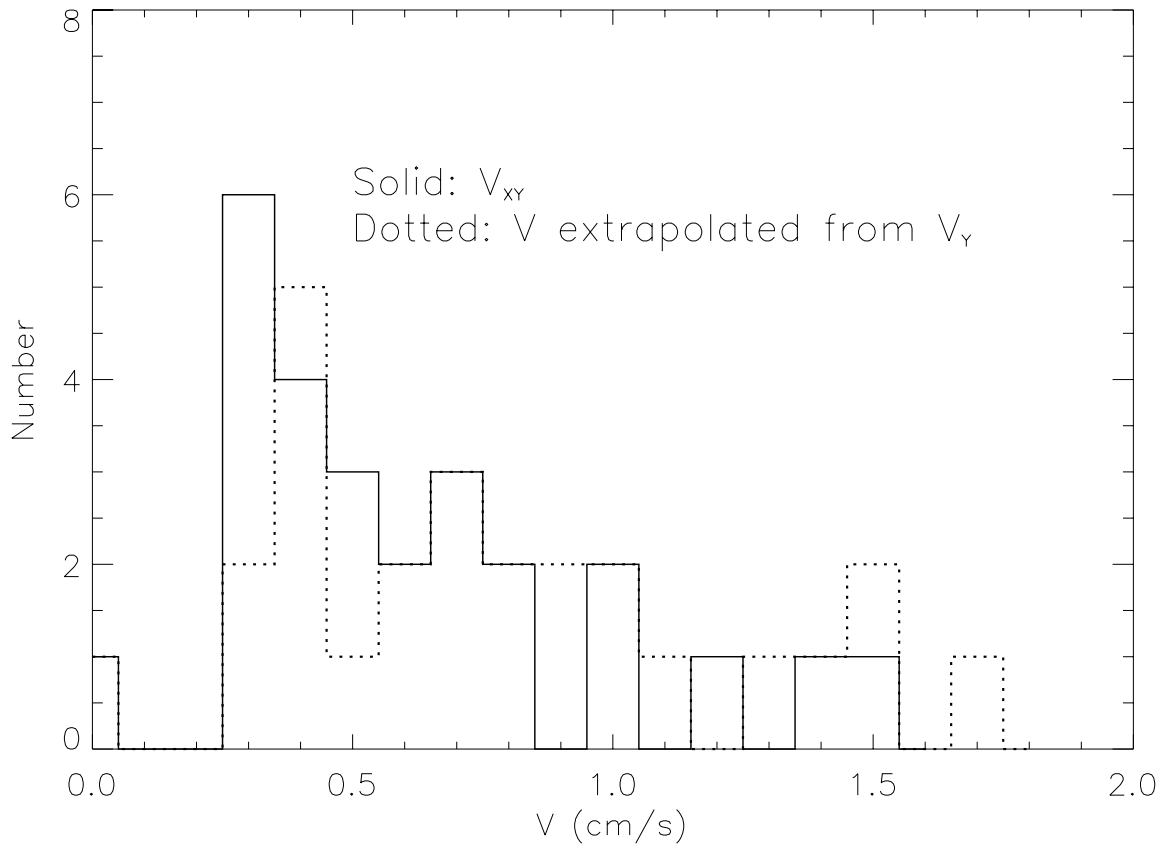


Figure 5: Distribution of the X-Y components of the ejecta in IBS 5 (solid), and distribution of velocities assuming that the ejecta launch angle is 45 degrees (dotted).

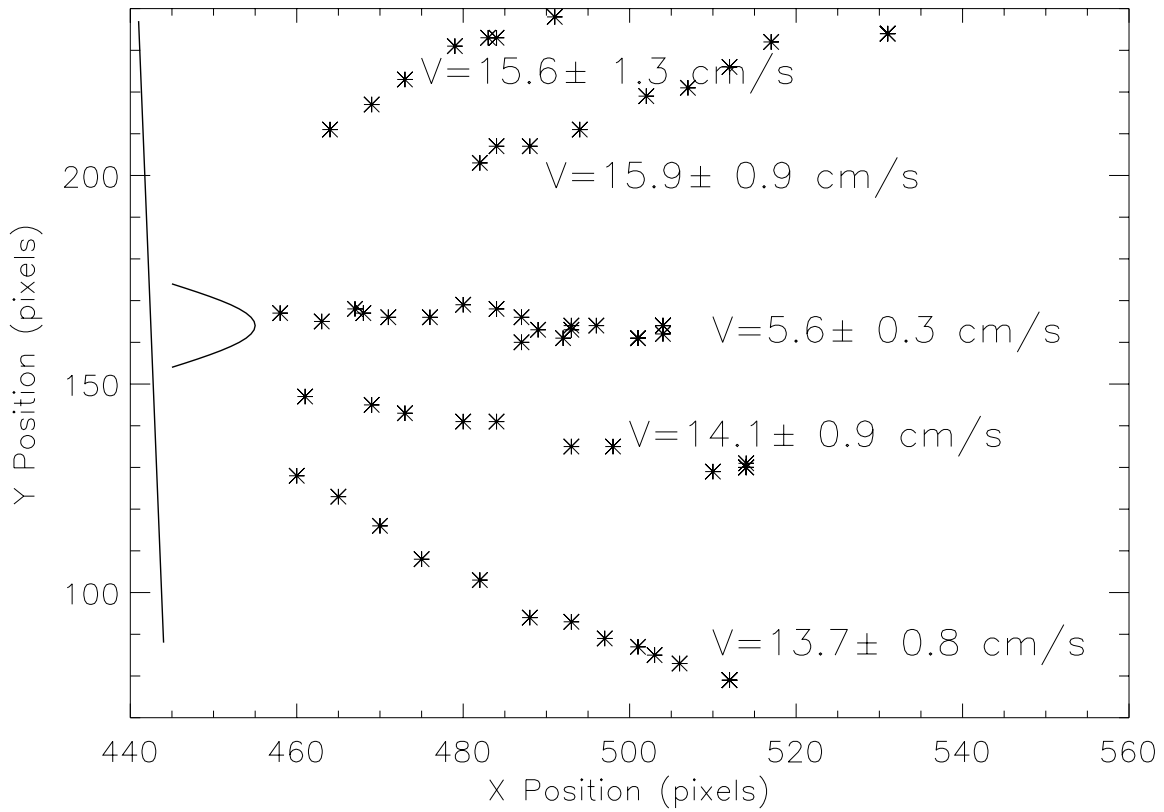


Figure 6: The target surface (line at left) and position and size of projectile at impact (curve at X=450, Y=165) for IBS 4 are plotted with the trajectories of five points along the ejecta curtain and the derived speeds for those points.



Figure 7: Three frame sequence at 0.5 second intervals from the impact in IBS 6 at 28 cm/s. The impact was slightly oblique (Table 2) leading to the asymmetric ejecta distribution seen here.